Building and Environment 103 (2016) 250–261

Contents lists available at ScienceDirect

Building and Environment

journal homepage: www.elsevier.com/locate/buildenv

An empirical model to predict the performance of typical solar chimneys considering both room and cavity configurations

Long Shi [a, *], Guomin Zhang [b]

[a] Centre for Environmental Safety and Risk Engineering, Victoria University, VIC 3029, Australia
[b] School of Civil, Environmental and Chemical Engineering, RMIT University, GPO Box 2476, Melbourne VIC 3001, Australia

ARTICLE INFO

Article history:
Received 14 January 2016
Received in revised form
20 April 2016
Accepted 20 April 2016
Available online 22 April 2016

Keywords:
Solar chimney
Natural ventilation
Computational fluid dynamics
Parametric analysis
Thermal buoyancy
Empirical model

ABSTRACT

The solar chimney is a reliable passive ventilation system that can largely reduce the energy requirements with both low costs and maintenance for buildings to overcome the current energy crisis. To optimize its design, an empirical model is developed to predict the performance of typical solar chimneys considering both room and chimney cavity configurations using easily acquired inputs. Fire Dynamics Simulator (FDS) as an excellent and open-source tool to solve heating, ventilation and air conditioning problems is selected for this study. The numerical modelling of FDS was first validated by previous experimental data, and then used to develop the empirical model. In this model, a coefficient describing room and chimney configuration (e.g., room opening, inlet and outlet of cavity) is proposed. It is shown that room size (length, width and height) and opening location have limited influence on performance. Also the radiation from hot walls can be ignored when compared to convection heat transfer between the hot walls and the air inside the cavity. This study provides key knowledge to optimize the design of solar chimneys in energy saving for buildings.

1. Introduction

Architects and building engineers are highly interested in exploring ways of ventilating buildings by passive means because of the problems raised by the energy crisis. The solar chimney (essentially a solar energy absorber with open top and bottom) is an excellent passive ventilation system and has been used for centuries to solve the ventilation problem [1]. A solar chimney in a single-story building can reduce annual total fan shaft power requirements by 50% [2]. It is increasingly proposed as an alternative to mechanical ventilation systems because of the potential benefits in operational costs, energy requirements, and carbon dioxide emissions [3,4]. Its main function is to provide natural ventilation to the building through solar induced air motion [5].

Previous studies have largely focused on the configuration of the solar chimney itself, ignoring the influence of the room and its openings. Their investigations are based on simplified two-dimensional (2D) models or a three-dimensional (3D) chimney cavity. The principle of designing a solar chimney is to maximize ventilation by maximizing solar gain, thereby creating a sufficient temperature (or pressure) difference between the inside and outside which then drives the air flow [3]. A big portion of solar chimney studies are aimed at finding optimum design solutions for enhancing natural ventilation, taking into consideration different design parameters, such as height [6,7], width and depth of cavity [8], chimney position [9], type of glazing [10], type of absorber [11,12], and the inclusion of insulation or thermal mass in the solar chimney [13,14].

Many analytical/mathematical models have been developed to predict the performance of solar chimneys under different situations. Andersen [15] developed an analytical model to predict natural ventilation by thermal buoyancy in a chimney cavity with two vertical openings. Bansal et al. [16] developed a mathematical model for a solar chimney considering different sizes of opening varying discharge coefficients. The effect of chimney inclination angle on indoor air flow was analytically investigated by Bassiouny and Korah [17]. However, one of the disadvantages of analytical models is that their practical applications seem to be hampered if they require lots of inputs that are hard to acquire, such as discharge coefficient [18], inlet and outlet pressure loss coefficient

* Corresponding author.
E-mail addresses: shilong@mail.ustc.edu.cn, long.shi@vu.edu.au (L. Shi).

http://dx.doi.org/10.1016/j.buildenv.2016.04.024
0360-1323/

Nomenclature

A	area (m^2)
C	coefficient (dependent on equation)
D	diffusivity (m^2/s)
E	specific enthalpy of material (J/kg)
g	acceleration of gravity (m/s^2)
h	heat transfer coefficient ($W/m^2 \cdot K$)
H	height (m)
I	radiation intensity
k	thermal conductivity ($W/m \cdot K$)
L	length (m)
$\dot{m}''$	mass flow rate ($kg/m \cdot s$)
P	pressure (Pa)
$\dot{q}''$	air flow rate (m^3/s)
$\dot{Q}''$	heat flow rate (W/m^2)
s	unit vector of radiation intensity
$\dot{S}''$	source term (dependent on equation)
t	time (s)
T	temperature (°C)
U	velocity (m/s)
U	integrated radiation intensity
V	volume (m^3)
W	width (m)
x, y, z	coordinate (m)

Greek letters

ε	emissivity (−)
k	absorption coefficient (m^{-1})
Δ	change in variable value (−)
ρ	density (kg/m^3)
σ	Stefan-Boltzmann constant ($W/m^2 \cdot K^4$)
τ	viscous stress tensor
ω	wavenumber of thermal radiation

Subscripts and Superscripts

0	ambient condition
b	blackbody
c	control volume
conv	convection
d	discharge
hot	hot wall
i	gas species
in	inlet
m	mass
n	neutral plane
open	opening
out	outlet
rad	radiation
r	ratio between inlet and outlet
R	room
sc	solar chimney

[19], and wall friction coefficient [7].

Numerical modelling plays an important part in investigating the performance of solar chimneys given the high cost of experiments [3,20–22]. A study by Chen [23] indicated that 70% of the literature used computational fluid dynamics (CFD) to study indoor air quality, natural ventilation and stratified ventilation because they are difficult to be predicted by other models. Bacharoudis et al. [24] carried out a 2D numerical investigation of the thermo-fluid phenomena inside solar chimneys by using FLUENT. Lee and Strand [4] developed a module implemented in the EnergyPlus program to address the effects of the chimney height, solar absorptance of the absorber wall, solar transmittance of the glass cover and the air gas width on solar chimneys. A CFD analysis based on the finite volume method was utilized to predict the thermal performance and fluid flow in 2D solar chimneys to identify the effect of different parameters [11].

Although CFD modelling can be used to predict the performance of solar chimneys, they are not as convenient as analytical models that can show the clear trends of influencing factors in practical applications. Analytical models can also accelerate prediction without requiring a long calculation time like CFD modelling. However, the related analytical analysis is difficult for prediction in complicated situations, such as multiple openings or changeable room volumes, as the method cannot predict the air movement in the whole room or targeted domain [25]. It is still unclear what the design parameters should be, and guidelines for meeting the ventilation requirements are unavailable [3].

Therefore, this study provides a comprehensive investigation on the performance of a typical solar chimney. Parameters regarding chimney and room configuration and cavity materials were analysed to develop an empirical model to predict the air flow rate of solar chimneys under various scenarios with easily acquired inputs. It will benefit the design of solar chimneys to save energy for buildings.

2. Methodology

2.1. A computational fluid dynamic model

A CFD software, Fire Dynamics Simulator (FDS) [26], was used to simulate the air flow in the solar chimney. It has been largely used to building professionals [27–30]. The reason for using FDS is because it is an efficient program to construct the model, even for complicated multiple-storey buildings. Although FDS focuses on fire related simulation, it is an excellent and open-source tool to solve heating, ventilation and air conditioning (HVAC) problems considering all the necessary aspects, such as turbulent flow, thermal radiation and conduction, particles and buoyancy. Large eddy simulation (LES) algorithm is implemented in the program, which can reduce the magnitude of the work by filtering out small length scales of flow without decreasing modelling accuracy. It is useful for the simulation of large-scale domain, such as multi-storey buildings. In LES, the “turbulence model” refers to the closure for subgrid-scale (SGS) flux terms and gradient diffusion is the turbulence model used to close both the SGS momentum and scalar flux terms [31]. The turbulent diffusivity is obtained using a constant Schmidt number (for mass diffusivity) or Prandtl number (for thermal diffusivity).

FDS considers many turbulence models, such as constant coefficient Smagorinsky model, dynamic Smagorinsky model, Vreman's model and renormalization (RNG) group model. The default to describe the turbulent viscosity is the Deardorff's model. This was selected based on comparisons with a wide variety of full-scale experiments. The computational domain in FDS is three dimensional.

The above features of FDS enable it to easily simulate the complicated situations with different building plans, even for complex buildings. For completeness, some features of FDS including the governing equations are introduced below.

The continuity equation is expressed by:

$$\frac{\partial \rho}{\partial t} + \nabla \cdot (\rho u) = \dot{S}''_m \tag{1}$$

The momentum equation is given by:

$$\frac{\partial u}{\partial t} - u \times \omega + \nabla \tilde{P} - P\nabla(1/\rho) = \frac{1}{\rho}[(\rho - \rho_0)g + \nabla \cdot \tau] \tag{2}$$

where $\tilde{P}$ is the total pressure divided by the density.

The energy conservation equation is written as:

$$\frac{\partial}{\partial t}(\rho E) + \nabla \cdot (\rho E u) = \frac{D\overline{P}}{Dt} - \nabla \cdot \dot{Q}'' \tag{3}$$

where $\dot{Q}''$ represents the conductive, diffusive, and radiative heat fluxes:

$$\dot{Q}'' = -k\nabla T + \dot{Q}''_{rad} \tag{4}$$

The net contribution from thermal radiation in the energy equation is expressed by:

$$\dot{Q}''_{rad} = \kappa(x)[U(x) - 4\pi I_b(x)]; \;\; U(x) = \int_{4\pi} I(x,s)ds \tag{5}$$

where $\kappa(x)$ is the absorption coefficient, m^{-1}; $I_b(x)$ is the source term; and $I(x,s)$ is the solution of the radiation transport equation (RTE) for a non-scattering gray gas:

$$s \cdot \nabla I(x,s) = \kappa(x)[I_b(x) - I(x,s)] \tag{6}$$

To solve the above governing equations, the LES algorithm was used. The LES equations are derived by applying a low-pass filter of width Δ to the above governing equations. The filter width is taken to be the cube root of the cell volume, $\Delta = V_c^{1/3}, V_c = \delta x \delta y \delta z,$. Then for any continuous field, ϕ, a filtered field is defined as:

$$\overline{\phi}(x,y,z,t) \equiv \frac{1}{V_c} \int_{x-\delta x/2}^{x+\delta x/2} \int_{y-\delta x/2}^{y+\delta y/2} \int_{z-\delta z/2}^{z+\delta z/2} \phi(x',y',z',t)dx'dy'dz' \tag{7}$$

In FDS, all the solid surfaces are considered to have thermal boundary conditions. Heat and mass transfer near the solid surfaces is described by empirical models. FDS uses a simple, direct-forcing immersed boundary method (IBM) for block Cartesian geometries. The default boundary condition for tangential velocity is based on a log law wall for both smooth and rough walls. Open boundary refers to the non-solid exterior boundary of the computational domain, at which gases are allowed to flow freely in and out depending on the local pressure gradient.

Because of the non-linear differential equation for pressure-velocity coupling, iteration is utilized to solve the problem until a successful convergence check, including the solution checks for errors in mass conservation, flow reversal over the time step and the magnitude of change for velocity. The default velocity tolerance is $0.5\delta x$, where δx is the characteristics grid cell size. Default error tolerance in units of atoms for the reaction stoichiometry is 10^{-5}, and for reaction stoichiometry mass balance is 10^{-4}. The user also can control the error tolerance and maximum number of iteration. Further details about FDS and mathematical models can be seen in McGrattan et al. [31].

2.2. Experiments for the validation

To validate numerical modelling of FDS, previous experimental setup and data were used [32]. Experiments were taken in a wooden room with dimensions of 1.7 m (long) × 1.9 m (wide) × 2.0 m (high). The testing environment is considered to be steady state, which was taken in a large enough building (20 m long, 10 m wide and 5 m high). The ambient air temperature kept at 20 °C in the building. Heat loss from the apparatus was reduced using 50 mm thick insulation sheets. The walls forming the cavity were of 2 mm aluminium sheet textured with a layer of sand. The inner surface of the cavity were heated by horizontal electrical heaters with the outer faces insulated and the heaters were mounted behind the plates at a distance of 50 mm so that the radiation heat input was well distributed on the cavity surface. The separation of the walls of the cavity, the sizes of the air inlet to the cavity and the window were variable to study their effect on the rate of air flow. Further details about experimental setup and procedure are described by Bouchair [32].

The computational model of the room and chimney cavity constructed by FDS is shown in Fig. 1. A moveable wall on the right hand side is used to construct different width cavities together with the right wall. Two hot surfaces are on the right side of the right wall and the left side of the movable wall, respectively. The width of the air inlet is 1.4 m and its height changes in order to study its influence on air flow. Transparent left and front walls in this figure are used to show the room interior, but do not imply that these two walls are transparent in term of properties that allows the radiation heat to go through directly. A window is located at the centre of the left wall with a size of 0.5 m (width) × 0.6 m (height).

As the details about the thickness of wall were not given in experiments [32], the thickness of floor, and walls constructing the cavity was assumed to be 0.2 m. The thickness of the other walls was then assumed to be 0.05 m. The length of the solar chimney cavity is fixed at 1.5 m. Following the experimental conditions, all the walls were assumed to be following inert boundary condition except the two walls constructing the chimney cavity, namely the two hot surfaces. The surfaces of cavity walls were set to specific temperature following the experiments. Ambient temperature for numerical modelling is the same with experiments, namely 20 °C.

During the simulation, an expanded domain showing grids was used in X, Y and Z directions to make sure the simulation was taking place in an ambient environment, shown in Fig. 1. For the validation part, a computational domain of 4.0 m (X) × 3.6 m (Y) × 3.6 m (Z) was used. For some cases in parametric analysis, such as a higher than 3.6 m cavity, the computational domain was also expanded when appropriate. The surrounding boundaries were considered to be open boundary conditions allowing the air to flow in or out under pressure difference, which is following the experimental setup. The grid in three dimensions can be seen in Fig. 1 as well, in which cubes were used for the control block and its size is dependent on the grid size.

In FDS, there is a default model for the description of convection heat transfer between the hot walls and surrounding air [31]. We have conducted a simulation of the solar chimney using the default model [33]. It is observed that the modelling results differ somewhat from the experiments. This may be because any kind of empirical model is based on specific test geometries with various kinds of focuses and limitations. For the targeted experiments [32], it was mentioned that the cavity walls were constructed of insulation board with polished aluminium on their internal faces, so the heat transfer coefficient of the two hot surfaces was assumed as 15 $W/m^2 \cdot K$, see also [34,35].

To examine grid independence, different mesh sizes were used in the numerical modelling. A case with inlet height of 0.4 m and surface temperature of 60 °C was chosen for this. The inlet air flow is an important output and was used to compare the modelling outputs under these three grid sizes, which can be given by:

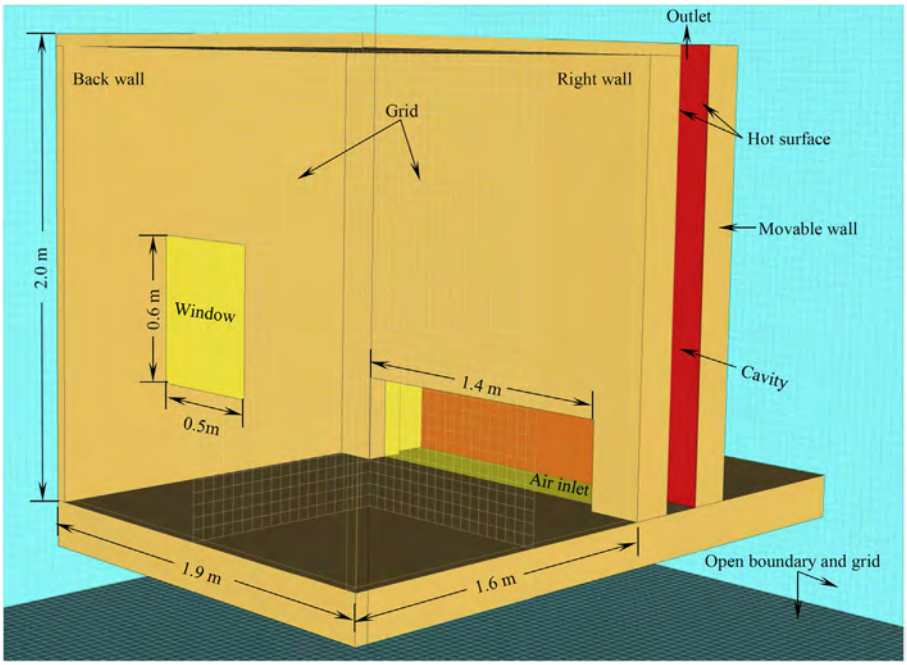

Fig. 1. The computational model of the room and solar chimney constructed by FDS. The size of window is 0.5 m (width) × 0.6 m (height); Width of air inlet is 1.4 m and the height is adjustable; the right wall and movable wall on the right hand side construct the chimney cavity; and the length of cavity is fixed at 1.5 m.

$$\dot{m}'' = u \cdot \rho \cdot A/L \tag{8}$$

Fig. 2 shows the inlet air flow within 100 s using different mesh sizes, including 0.10 m, 0.08 m, 0.05 m and 0.004 m. The CPU calculation time using these four grid sizes based on an Intel dual-core computer (3.0 GHz) are about 7 min, 15 min, 75 min and 200 min, respectively. It is observed from the figure that the air inlet flow decreases a little bit when grid size reduces from 0.10 m to 0.08 m, but it shows limited influence on the outputs when grid size is below 0.05 m, especially after the simulation approaches stable stage. This means that the grid size of 0.05 m can be considered as grid independent. In the subsequent modelling a grid size of 0.05 m will be utilized in x, y and z directions unless otherwise specified.

For the experiments conducted by Bouchair [32], the air inlet flow of the solar cavity, as an important parameter to determine the performance of solar chimney, were measured under the influences of cavity width, surface temperature and inlet height. The air inlet flow is the stable value when the flow achieves stable condition under specific surface temperature. These experimental data were used to validate the numerical modelling under various conditions. We did not compare the detailed numerical outputs, such as the air velocity at specific locations, as the original experiments did not provide such data.

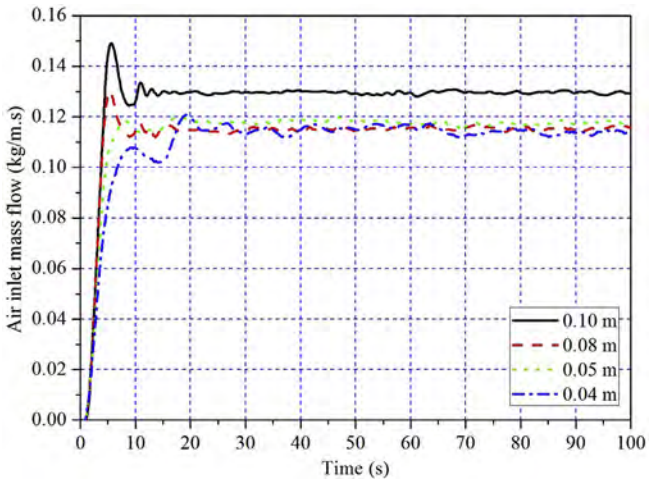

Fig. 2. Comparison of air inlet mass flow using different mesh sizes. X axis shows the time and Y axis represents the air inlet mass flow.

2.3. Validation of modelling

Scenarios with various air inlet heights, cavity widths and surface temperatures were included to validate the numerical modelling, shown in Table 1. It can be seen in Fig. 2 that the air inlet flow will approach a stable stage after a period of time. For typical cases, a modelling time of 50 s was utilized and the average air inlet flows during the last 10 s were compared with experiments. For the cases with 0.5 m and 1.0 m wide cavity, stabilizing the inlet air flow takes a little longer time so the modelling time under these scenarios were 100 s and 300 s, respectively, and air flows during the last 10 s were averaged for the comparison.

Fig. 3 shows air inlet flow stream with 60 °C hot surfaces at 50 s for a 0.2 m wide chimney cavity. The air in the room is driven by the pressure difference caused by the two hot surfaces. The temperature of the air between the two hot surfaces increases by convection, which is strongly dependent on the heat transfer coefficient of the wall materials. The pressure inside the cavity reduces as hot air rises under buoyancy. The reason for the pressure drop inside the cavity is the high temperature, according to the ideal gas law. Air inside the room then enters the cavity through the inlet under the pressure difference. At the same time, the outside air enters the room through the window, and the speed decreases a little along the flow path. After the air flow hits the wall, it splits into two streams: one goes up to the roof, blocked by the ceiling and goes back again; another goes down to the floor, then enters the cavity. It

Table 1
The scenarios and modelling parameters for the validation.

Item	Description	Symbol	Unit	Value
Solar chimney	Air inlet height	H_{in}	m	0.1, 0.4
	Cavity width	W_{sc}	m	0.1, 0.2, 0.3, 0.5, 1.0
	Surface temperature	T_{sc}	°C	30, 40, 50, 60
Modelling	Grid size	Δx	m	0.05
	Heat transfer coefficient	h	W/m^2·K	15 [34,35]
	Emissivity of wall	ε	–	0.15 [36]
	Computational domain	-	m	4.0 (wide) × 3.6 (long) × 3.6 (high)

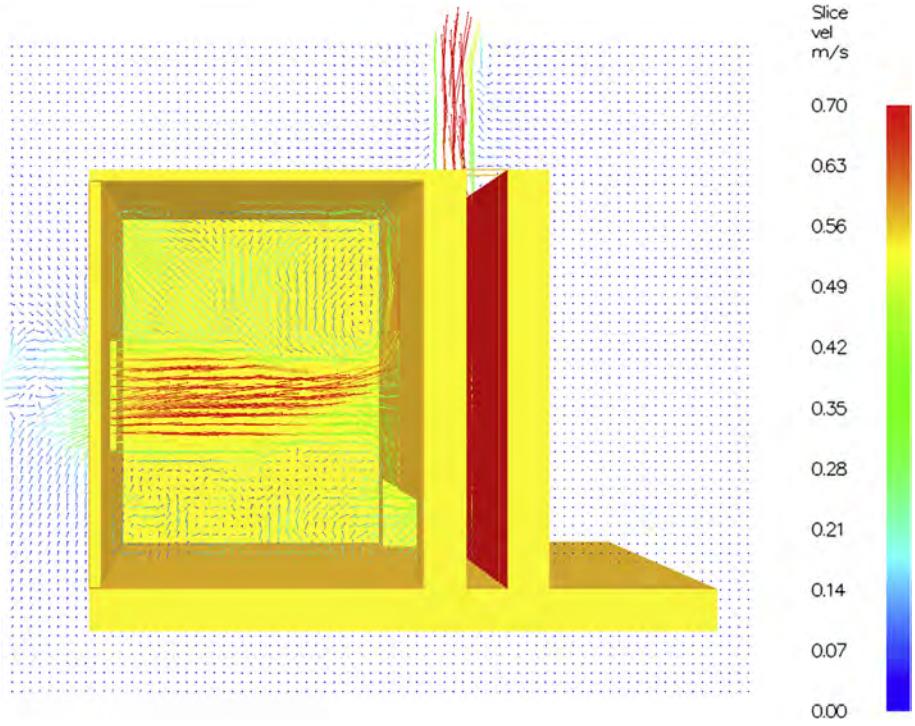

Fig. 3. The air flow of 0.2 m wide solar chimney cavity with 60 °C hot surface at 50 s. The colour bar on the right shows a velocity range of 0–0.7 m/s. (For interpretation of the references to color in this figure legend, the reader is referred to the web version of this article.)

is observed that the maximum air flow speed above the cavity is about 0.7 m/s when the two hot surfaces are at 60 °C, which is similar to the flow entering through the window. It should be noticed that the air flow at the top cavity was not calculated solely by the velocity of 0.7 m/s and the area. This is because a maximal velocity of 0.7 m/s does not represent the whole plane is under such air velocity. During numerical modelling, we used a built-in function to monitor the flow rate of the whole defined plane in FDS.

Fig. 4 shows the comparison between experiments and modelling outputs. Four surface temperatures (30 °C, 40 °C, 50 °C and 60 °C), two inlet heights (0.1 m and 0.2 m), and five cavity widths (0.1 m, 0.2 m, 0.3 m, 0.5 m and 1.0 m), were included in the comparison. In this figure, symbols represent the experimental results and the lines are the modelling outputs. It is observed that FDS can predict the air flow reasonably well under various scenarios. It is also noticed that modelling results are slightly lower than the experimental results for 1.0 m wide cavities, but the modelling shows the same trend as the experiments under the effect of hot surfaces.

It is noticed that convection heat between the air in the cavity and hot surface is the main source for the heating up. Take the 60 °C surface with a heat transfer coefficient of 15 W/m^2·K for example, the radiation heat and convection heat transfer are about 0.65 W/m^2 and 600 W/m^2, respectively, obtained from Eqs. (11) and (12). Therefore, the convection process takes the lead among these two heat sources. The convection process can be clearly identified at the beginning of modelling outputs, shown in Fig. 5.

3. Parametric analysis

3.1. Analytical model

The air flow rate under thermal buoyancy driven by temperature differences for a space with two different height openings can be expressed by Ref. [15]:

$$\dot{q}''_{in} = 0.037 C_d^{2/3} \left(\dot{Q}'' A_{hot} H_n \right)^{1/3} A_{in}^{2/3} \tag{9}$$

where H_n is the distance between the inlet centre and the neutral plane, m.

Air in the cavity is heated by two kinds of heat transfer methods, with the total heat input expressed by:

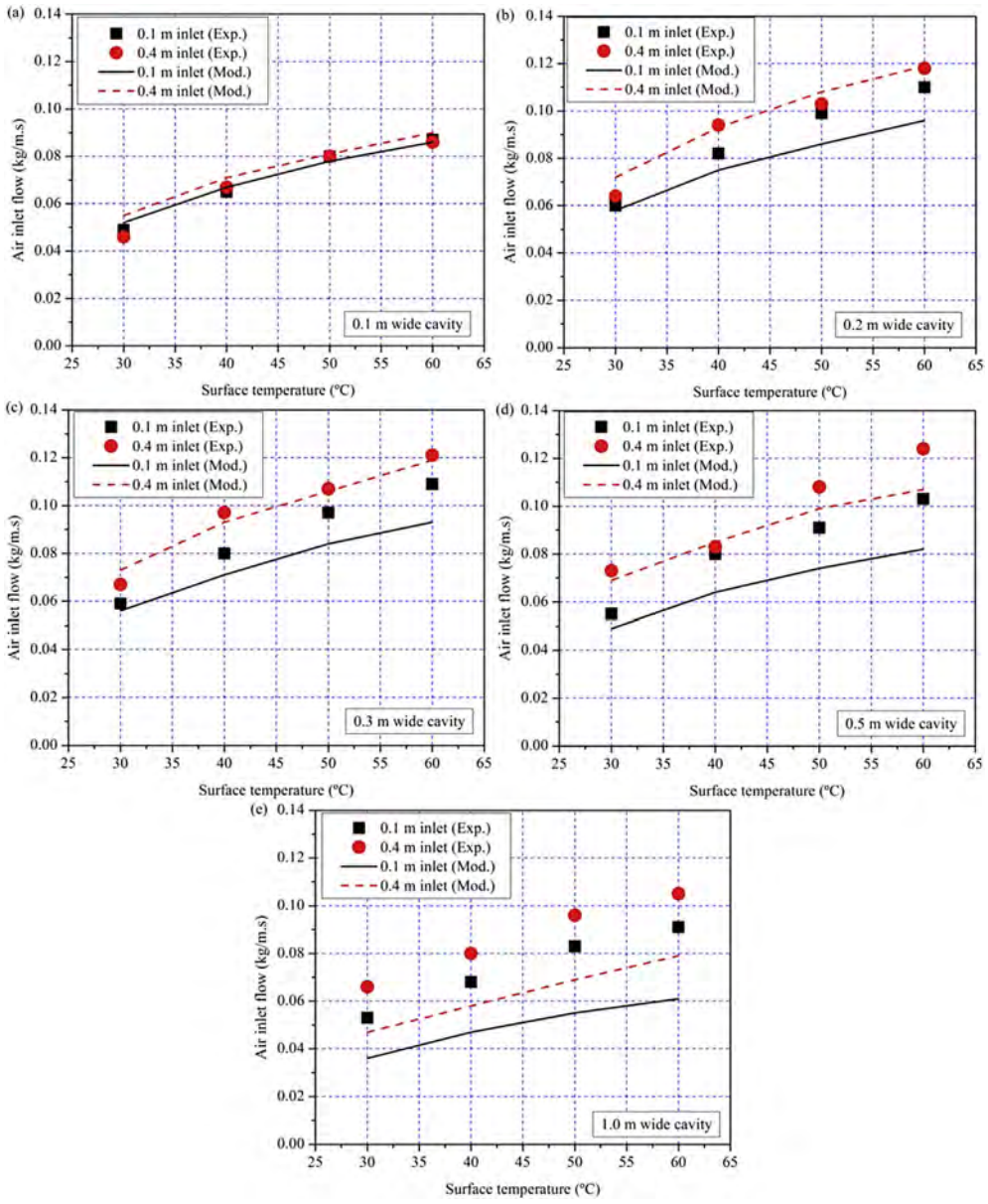

Fig. 4. Comparison between experiments and modelling for various cavity widths: (a) 0.1 m; (b) 0.2 m; (c) 0.3 m; (d) 0.5 m; and (e) 1.0 m. The symbols (circles and squares are for 0.4 m and 0.1 m high air inlet, respectively) are the experimental data and lines shows the numerical outputs. The low right corner of each subfigure shows the cavity width.

$$\dot{Q}'' = \dot{Q}''_{rad} + \dot{Q}''_{conv} \tag{10}$$

The radiation heat can be given by the Stefan-Boltzmann's law:

$$\dot{Q}''_{rad} = \varepsilon\sigma\left(T_{sc}^4 - T_0^4\right) \tag{11}$$

The convection heat transfer between the two different temperature surfaces can be obtained by Newton's law of cooling:

$$\dot{Q}''_{conv} = h(T_{sc} - T_0) \tag{12}$$

After inserting Eqs. (10)–(12) into Eq. (9), we obtain that:

$$\dot{q}''_{in} = 0.037C_d^{2/3}\left[\varepsilon\sigma\left(T_{sc}^4 - T_0^4\right) + h(T_{sc} - T_0)\right]^{1/3} A_{hot}^{1/3} H_n^{1/3} A_{in}^{2/3} \tag{13}$$

It can be seen from the above analysis that the radiation heat can be ignored when it is compared with the convection heat. So, Eq. (13) can be approximated by:

$$\dot{q}''_{in} = 0.037C_d^{2/3} \cdot \left[h \cdot A_{hot} \cdot H_n \cdot A_{in}^2 \cdot (T_{sc} - T_0)\right]^{1/3} \tag{14}$$

Eq. (14) can be utilized to predict the air inlet flow rate for a solar chimney. However, the prediction does not consider the room configuration, such as room size and the openings. The air inlet flow considering the room configuration can then be expressed by:

$$\dot{q}''_{in} = C \cdot \left[h \cdot A_{hot} \cdot H_n \cdot A_{in}^2 \cdot (T_{sc} - T_0)\right]^{1/3} \tag{15}$$

3.2. Installation of solar chimney

The whole parametric analysis is based on the original room

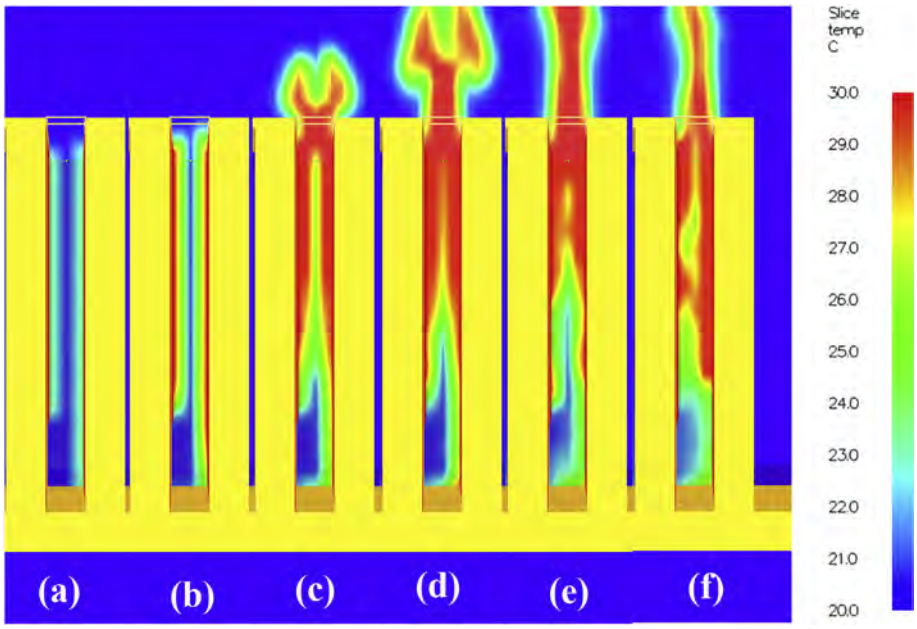

Fig. 5. The temperature in the 0.2 m wide cavity with a hot surface temperature of 60 °C along the time: (a) 1 s; (b) 2 s; (c) 4 s; (d) 5 s; (e) 20 s; and (f) 50 s. The colour bar on the right shows a temperature range of 20–30 °C. (For interpretation of the references to color in this figure legend, the reader is referred to the web version of this article.)

configuration, shown in Fig. 1, with a surface temperature of 60 °C and heat transfer coefficient of 15 W/m^2·K. Several chimney configuration parameters are investigated, such as air inlet height, air inlet width, cavity width and chimney height, as shown in Table 2. The interval in this table shows the increment for various scenarios.

In Eq. (15), the distance between the neutral pressure plane and the inlet centre, H_n, can be estimated by Ref. [15]:

$$H_n = \frac{H_{sc}}{1 + (A_{in}/A_{out})^2} \tag{16}$$

After combining Eq. (15) with Eq. (16), a proportional relationship can be gained between the inlet air flow rate and area of inlet and outlet,

$$\dot{q}''_{in} = C \cdot \left[\frac{A_{in}^2}{1 + (A_{in}/A_{out})^2} \right]^{1/3} \tag{17}$$

However, no linear relationship was found between $\dot{q}''_{in}$ and $[A_{in}^2/(1 + (A_{in}/A_{out})^2)]^{1/3}$ after inputting the data from the numerical modelling. This is probably because the H_n is used for the case where both inlet and outlet are vertical. When A_{out} increases with a higher cavity width, the air flow in the cavity is then turbulent, resulting in backward flow in the cavity. The process in the present study is significantly different with a vertical outlet. Therefore, a relationship between the inlet air flow and the area of inlet and outlet is then assumed to be,

Table 2
The parametric analysis of the installation of solar chimney.

Parameter	Symbol	Unit	Analysis range	Interval
Air inlet height	H_{in}	m	0.05–0.60	0.05
Air inlet width	W_{in}	m	0.3–1.5	0.1
Cavity width	W_{sc}	m	0.1–1.0	0.1
Chimney height	H_{sc}	m	1.2–3.2	0.2

$$\dot{q}''_{in} = C \cdot f(A_r) \tag{18}$$

where A_r is the ratio between A_{in} and A_{out}, which is given by:

$$A_r = A_{in}/A_{out} \tag{19}$$

Based on Eq. (18), the relationship between $\dot{q}''_{in}$ and A_r can be seen in Fig. 6. In this figure, the circles are the data from numerical modelling and the line is the regression line. It is observed these two agree reasonably well, with the equation for the regression line given by:

$$\dot{q}''_{in} = 0.16 - 0.009A_r - 0.025A_r^{-1} \tag{20}$$

Eq. (20) is consistent with practice. It is known that the air inlet flow increases under a higher A_{in}, but the increasing rate slows

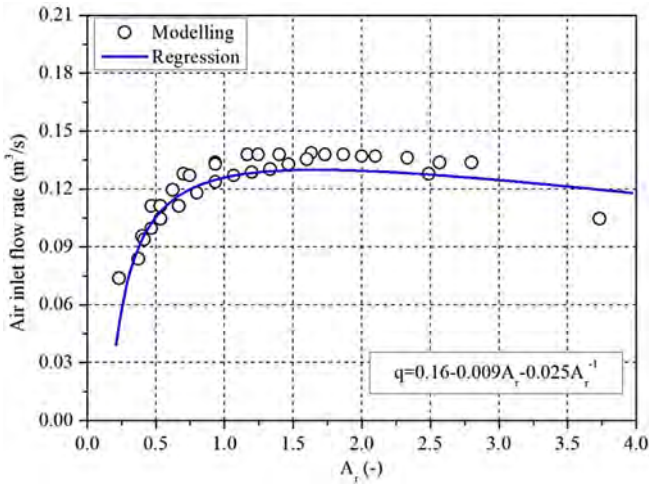

Fig. 6. The influence of inlet and outlet areas on the inlet air flow. Circles are numerical outputs and line is regression line.

down when A_{in} keeps rising. This is because the buoyancy flow keeps constant even though the air resistance produced by the inlet is decreasing. Inlet air flow increases with a higher A_{out}, but the air inlet flow decreases when A_{out} keeps rising, which is because a wider cavity increases the Reynolds number, then resulting in backward air flow. A similar phenomenon was also found in previous studies. Andersen [37] indicated that cavity width of solar chimney should be above 4.7 cm but less than 0.2–0.3 m as the maximum inlet flow happens during this range. Zhai et al. [38] observed backward air flow from experiments with a cavity width of 0.2 m.

A range of solar chimney height (1.2–3.2 m) was also investigated, shown in Table 2. The change of chimney height results in a change of area of hot surface (or wall), A_{hot}, as well. It is known from Eq. (15) that $\dot{q}''_{in}$ is linear to $(H_s A_{hot})^{1/3}$, which is reflected by the modelling outputs, shown in Fig. 7. The relationship is given by:

$$\dot{q}''_{in} = 0.06(H_{sc}A_{hot})^{1/3} \quad (21)$$

This result agrees well with the buoyancy flow, which is driven by pressure (or density) difference at different heights. According to the ideal gas law, air density decreases with a higher temperature. Similar results were also found from previous studies, for example, Lee and Strand [4] indicated that a higher solar chimney with great absorber wall resulted in a larger building natural ventilation.

3.3. Room configuration

To address the effect of room configuration on the air inlet flow, several parameters were considered, such as the area of the opening, width, length and height of the room, opening locations, and height of opening centre, as shown in Table 3. Openings in this study are not limited to windows, but also doors and skylights. An additional opening with the same size as the original window, namely 0.5 m × 0.6 m, was added in the middle of the front wall (window), back wall (window), roof (skylight) or back wall (door, which is located at the left corner near the left wall).

As shown in Eq. (15), $\dot{q}''_{in}$ is influenced by areas of inlet and outlet. The $\dot{q}''_{in}$ against the area of window (A_{open}) was addressed, shown in Fig. 8(a). It should be noted that the A_{open} in the numerical modelling varies by adjusting its width or height individually. So the cases in Fig. 8(a) reflect the trend of a single increase of window width or height. In Fig. 8(b), A_{open} increases by adjusting both width and height with an increment of 0.1 m from the original size (0.5 m × 0.6 m) until the left wall is totally replaced by window (or opening) (1.8 m × 1.95 m).

It can be seen from Fig. 8 that both situations result in the same trend along $\dot{q}''_{in}$ in that it increases dramatically with A_{open} initially but the rate of increase then slows down. The trend can be given by:

$$\dot{q}''_{in} = A_{open}/(0.65 + 5.2A_{open}) \quad (22)$$

Eq. (22) reflects the air resistance (or pressure difference) as air flows in to the room through the window, then is exhausted by the chimney cavity.

Fig. 9 shows the influence of room configuration (width, length and height of room, location of opening and height of opening centre) on air inlet flow rate. It is observed that the room size has limited influence on $\dot{q}''_{in}$, which stays at 0.137 m^3/s for various room sizes, shown in Fig. 9(a)–(c). It indicates that the room size has limited resistance on the air flow. The pressure between the inside and outside could be the same when the room size changes, indicating that the whole room can be considered as a control volume for future analytical analysis. As the window is located on the left wall, the length of room also reflects the distance from the opening to the air inlet, shown in Fig. 9(a). This shows that this distance has limited effect on air inlet flow.

The effect of additional openings on $\dot{q}''_{in}$ can be seen in Fig. 9(d). The flow $\dot{q}''_{in}$ is higher than those data from Fig. 9(a)-(c) because there is an additional opening compared to the original setup. Similarly, the $\dot{q}''_{in}$ did not vary too much with different locations of opening. However, the skylight in the roof shows a slightly higher value than the others.

The height of the opening centre was also addressed, shown in Fig. 9(e). It is observed that the $\dot{q}''_{in}$ tends to increase with a lower opening position. This is because the air flow from a lower opening enters the solar chimney more easily under similar height. The air flow could be smoother without going through vortexes by bouncing from the wall and then entering the cavity. Details of the whole process can be seen in Fig. 3. Although the $\dot{q}''_{in}$ seems to increase with a lower opening, the whole variation is less than 0.014 m^3/s even when the opening moves from the very top to the very bottom on the left wall, which means that the difference induced by the opening location can be ignored.

From the above analysis, it can be concluded that:

$$\dot{q}''_{in} = Constant\ (W_R, L_R, H_R, Opening\ location, H_{open}) \quad (23)$$

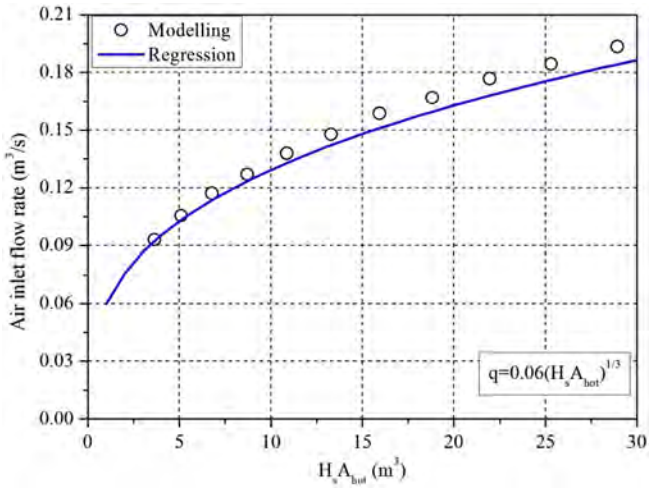

Fig. 7. The influence of chimney height on the air inlet flow. Circles are numerical outputs and line is regression line.

3.4. Influence of cavity materials

Cavity material is also an important aspect related to the performance of the solar chimney as it affects the heat gained from radiation. To address the influence of cavity material, characteristics of wall materials such as surface temperature (absorption of solar radiation), heat transfer coefficient and emissivity were included, shown in Table 4.

Surface temperature under solar radiation can be calculated by its absorption coefficient and thermal conductivity if the material is not transparent. The accumulated heat inside the wall is a balance between the absorption of solar radiation and thermal conductivity. The details about the calculation process are given in Bassiouny and Koura [39], in which an empirical model was developed to predict the average temperature of a solar absorber. Based on Eq. (15), $\dot{q}''_{in}$ is linear in $(T_s - T_0)^{1/3}$, which has been confirmed by the data from numerical modelling, shown in Fig. 10(a). The relationship can be given by:

Table 3
The parametric analysis of the Configuration of room.

Parameter	Symbol	Unit	Analysis range	Interval
Width of window	L_{open}	m	0.1–1.0	0.1
Height of window	H_{open}	m	0.1–1.0	0.1
Length of room (Distance of opening)	L_R	m	0.4–4.0	0.4
Width of room	W_R	m	0.6–4.2	0.3
Height of room	H_R	m	1.2–3.2	0.2
Opening location	-	–	windows, skylight, door	–
Height of opening centre	H_{open}	m	0.3–1.5	0.2
Area of opening	A_{open}	m^2	0.49–3.51	Length and height increase by 0.1 m

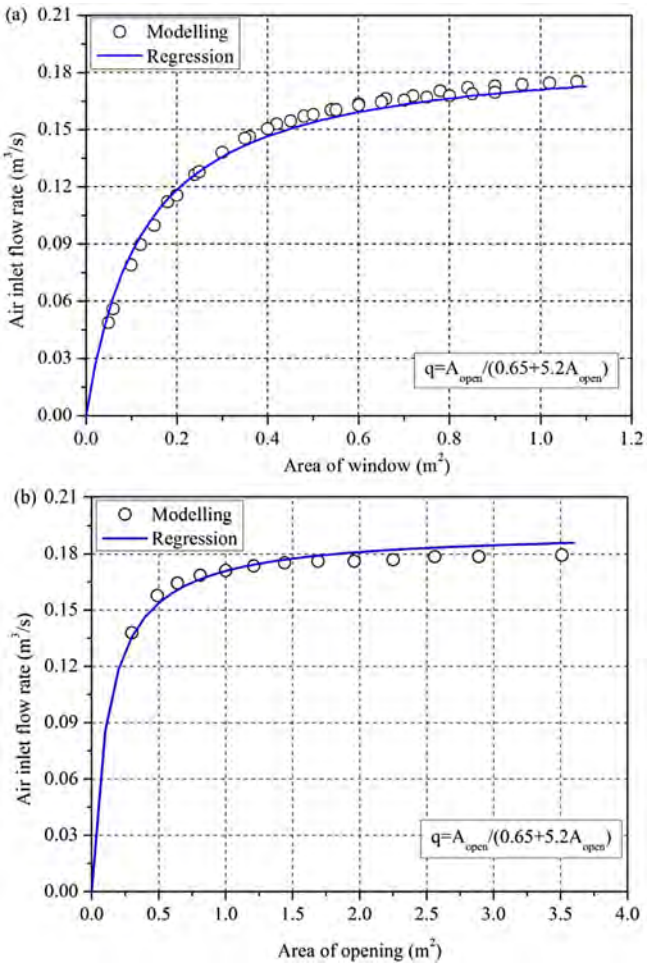

Fig. 8. The influence of opening on the air flow rate: (a) area of window; and (b) area of opening. Circles are numerical outputs and line is regression line. In (a), the opening area varies by adjusting its width or height individually; and in (b) the opening area varies by adjusting both width and height from the original size until the left wall is totally replaced by window/opening.

$$\dot{q}''_{in} = 0.04(T_{sc} - T_0)^{1/3} \tag{24}$$

Fig. 10(b) shows the relationship between $\dot{q}''_{in}$ and h, which is similar to the surface temperature in that $\dot{q}''_{in}$ increases exponentially with increasing h. As discussed above, the convection heat transfer is the main heating source for the air inside the cavity to lift the air under the buoyancy. The relationship can be expressed by:

$$\dot{q}''_{in} = 0.056h^{1/3} \tag{25}$$

The emissivity of the wall material related to the radiation heat absorption from the high temperature wall was also included. Not surprisingly, the emissivity has limited effect on the performance of the solar chimney, as shown in Fig. 10(c). The reason has been provided above in that the radiative heating by the hot wall can be ignored when compared with the convective heating. For hot wall radiation, $\dot{q}''_{in}$ is given by:

$$\dot{q}''_{in} = Constant\ (\varepsilon) \tag{26}$$

Eq. (26) only implies that the performance of the solar chimney is not affected by emissivity in the aspect of radiation from the hot wall, but this does not mean that the emissivity of cavity materials is not important for the performance under other radiation sources, such as the sun. The material with a higher emissivity would be prone to absorb more solar radiation, resulting in higher temperature walls. As this study is focused on the performance based on a specific temperature of the cavity wall, the emissivity in this study is then related to the wall radiation, not the solar radiation. Details about the solar absorption can be found in Harris and Helwig [40].

3.5. Empirical model

In the above sections, the effects of cavity and room configuration and thermal properties of cavity materials on the performance of chimney have been addressed. It is shown that the area of opening, inlet, outlet, hot wall, heat transfer coefficient, chimney height and surface temperature influence performance. Some other parameters regarding room configuration (e.g., room size, opening location, opening height) show very limited influence. In the aspect of heat gained by hot wall, emissivity of cavity materials did not affect the performance much.

After combining Eq. (15) and Eqs. (20)–(26), the air inlet flow based on a specific temperature wall can be expressed by:

$$\dot{q}''_{in} = \frac{C_1 + C_2A_r + C_3A_r^{-1}}{C_4 + C_5A_{open}^{-1}}[h \cdot H_{sc} \cdot A_{hot} \cdot (T_{sc} - T_0)]^{1/3} \tag{27}$$

The coefficients in Eq. (27) can be obtained by inputting the data from the numerical modelling in this study. An empirical model was then developed to predict the air inlet flow under various situations:

$$\dot{q}''_{in} = C_R \cdot [h \cdot H_{sc} \cdot A_{hot} \cdot (T_{sc} - T_0)]^{1/3} \tag{28}$$

where C_R is the room configuration coefficient related to room openings, chimney inlet and outlet.

$$C_R = \frac{0.1 + 0.0016A_r - 0.003A_r^{-1}}{9.9 + 1.5A_{open}^{-1}},\ where\ A_r = \frac{A_{in}}{A_{out}} \tag{29}$$

Fig. 11 shows the comparison between the experimental data

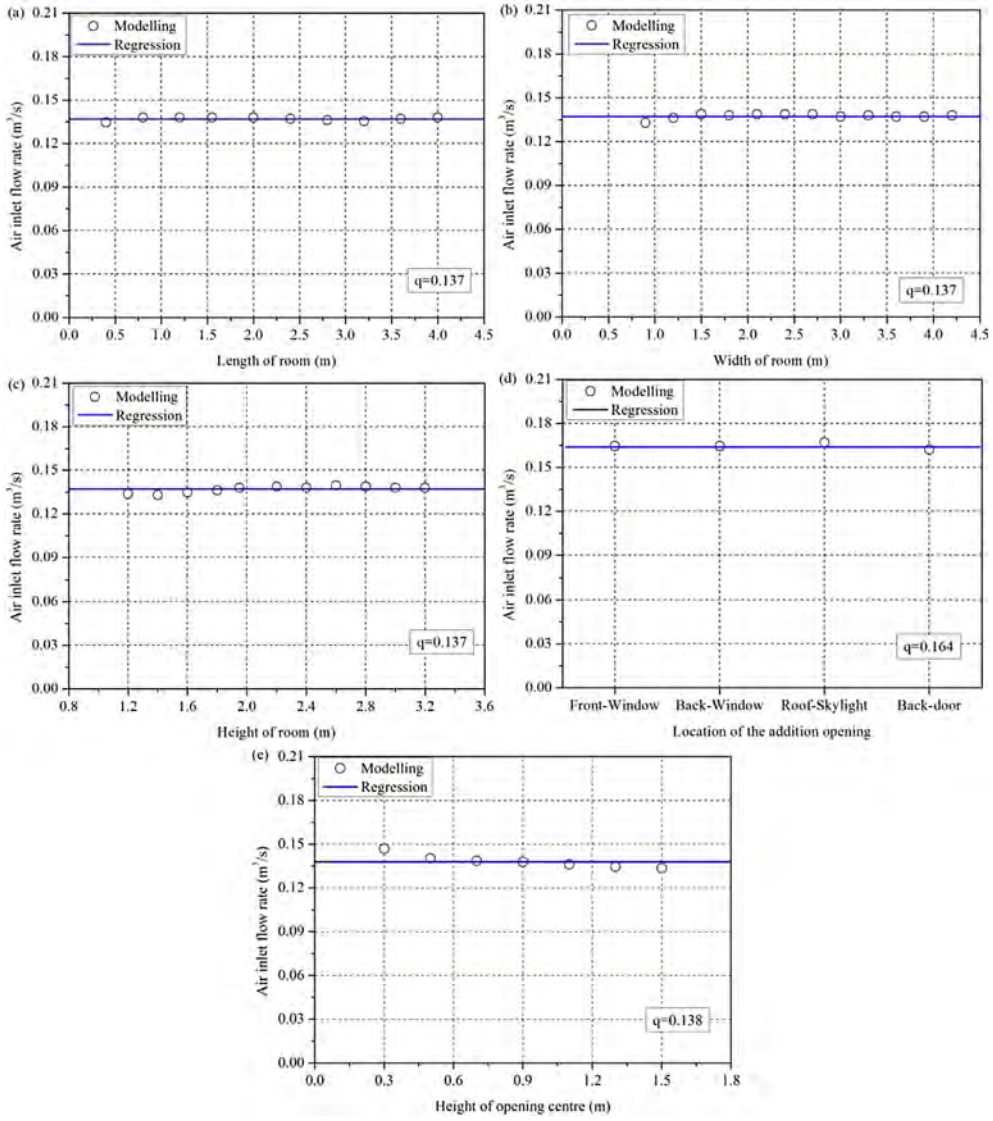

Fig. 9. The influence of room configuration on the inlet air flow: (a) Length; (b) Width; (c) Height; (d) opening location; and (e) height of opening. Circles are numerical outputs and line is regression line.

Table 4
The parametric analysis of the cavity materials.

Parameter	Symbol	Unit	Analysis range	Interval
Surface temperature	T_{sc}	°C	25–80	5
Heat transfer coefficient	h	W/m^2·°C	3–30	3
Emissivity	ε	–	0–1.0	0.1

[32] and numerical modelling in this study using Eq. (28). It can be seen that the prediction agree reasonably well with both the experimental and numerical data. The comparison between the prediction and experiments shows that the maximum and minimal differences are 55.4% and 0.24%, respectively, with an average difference of 10.9%. The big difference between these two are due to the eight predictions for 1.0 m wide solar cavity, with a range of errors of 23.4–55.4%. If we ignore the cases for a 1.0 m wide solar cavity, the maximum and minimal differences between the prediction and experiments then drop to 17.7% and 0.24%, respectively, with an average difference of 7.6%. From this figure, it is observed that the predictions of eight points for 1.0 m wide cavity are much lower than the experiments, which is similar to those cases in the validation part. This extreme situation of wide solar cavity will be a focus in our future study.

4. Conclusions

An empirical model was developed to predict the performance of typical solar chimneys considering both room and chimney configurations using easily acquired inputs. An open-source tool, Fire Dynamics Simulator (FDS), was selected and validated by the experimental data. It is observed from the comparisons that FDS can predict the air inlet flow of solar chimney quite well with various inlet heights, chimney widths and surface temperatures, except the numerical results for 1.0 m wide cavity are a little lower than the experiments. Based on the numerical modelling, the influences of room and cavity configurations and cavity materials properties on the inlet flow rate of solar chimney were addressed:

(1) The air inlet flow rate increase with bigger inlet or outlet areas and chimney height, however, the increasing rate slows

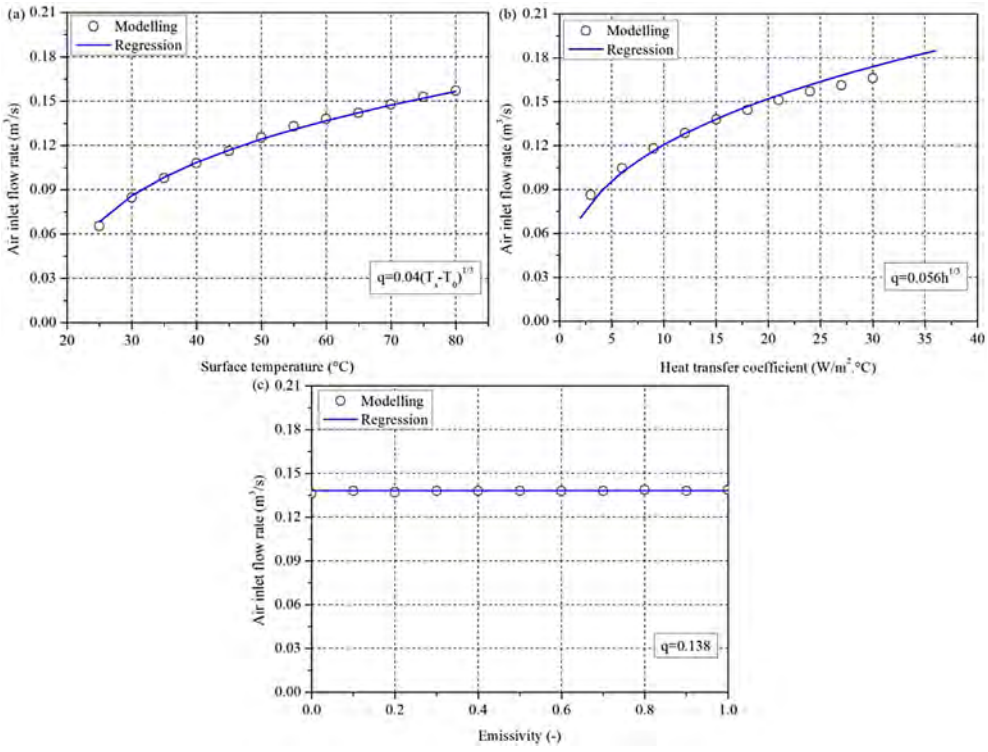

Fig. 10. The influence of cavity material properties on air inlet flow: (a) Surface temperature; (b) heat transfer coefficient; and (c) Emissivity. Circles are numerical outputs and line is regression line.

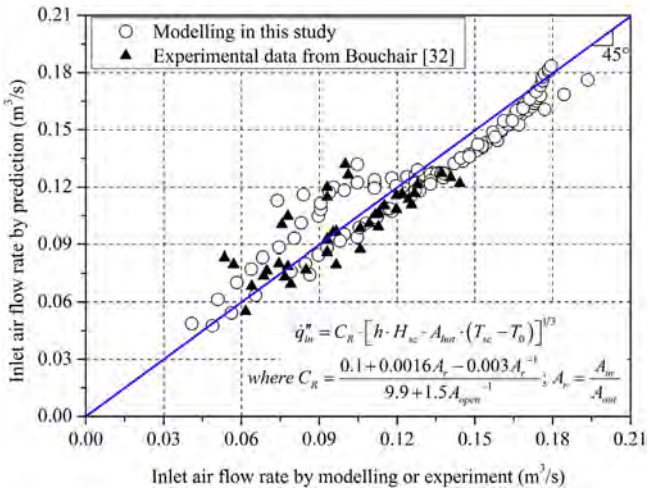

Fig. 11. Comparison of inlet air flow between experimental and numerical data and empirical model. Open circles are numerical outputs, filled triangles are experimental data [32] and the 45° line represents the equivalence between X and Y data.

down when they keep rising. For the outlet, the air inlet flow rate decreases when its area continues rising, which is because a wider cavity could bring in backward air flow under high Reynolds number.

(2) It is observed that the room size (e.g., length, width and height) has limited effect on the air inlet flow. This indicates that the whole room space can be considered as a single control volume for future analytical analysis. The air inlet flow of solar chimney seems to increase under a lower opening position, but its effect can be ignored as the variation when the opening moved from the very top to the very bottom on the left wall is negligible. The air inlet flow rate rises with a bigger opening, but the flow seems to approach a maximum value. It is obtained that:

$$\dot{q}''_{in} = Constant\ (W_R, L_R, H_R, Opening\ location, H_{open})$$

(3) A cavity material which results in a higher temperature can optimize the chimney performance. For a specific wall temperature, the convective heat transfer between the wall and the air inside the chimney cavity is the leading source for the buoyancy flow.

(4) In the empirical model, a room coefficient (C_R) is proposed to describe the influence of both the room and chimney configurations on the inlet air flow of the solar chimney. The empirical model can be expressed by:

$$\dot{q}''_{in} = C_R \cdot [h \cdot H_{sc} \cdot A_{hot} \cdot (T_{sc} - T_0)]^{1/3}, \quad where\ C_R = \frac{0.1 + 0.0016A_r - 0.003A_r^{-1}}{9.9 + 1.5A_{open}^{-1}};\ A_r = \frac{A_{in}}{A_{out}}$$

In this study, FDS was used to predict the performance of solar chimney using large eddy simulation (LES) algorithm. We believe the influence of turbulence models on the modelling accuracy will be a very good topic for future research.

Acknowledgements

The authors would like to thank Dr. Kevin McGrattan at U.S. National Institute of Standards and Technology (NIST) for the valuable help about the validation of Fire Dynamics Simulator (FDS) on simulating the solar chimney performance.

References

[1] P. Lotfabadi, Analyzing passive solar strategies in the case of high-rise building, Renew. Sustain. Energy Rev. 52 (2015) 1340–1353.
[2] T. Miyazaki, A. Akisawa, T. Kashiwagi, The effects of solar chimneys on thermal load mitigation of office buildings under the Japanese climate, Renew. Energy 31 (2006) 987–1010.
[3] R. Khanal, C.W. Lei, Solar chimney – a passive strategy for natural ventilation, Energy Build. 43 (2011) 1811–1819.
[4] K.H. Lee, R.K. Strand, Enhancement of natural ventilation in buildings using a thermal chimney, Energy Build. 41 (2009) 615–621.
[5] B. Zamora, A.S. Kaiser, Numerical study on mixed buoyancy-wind driving induced flow in a solar chimney for building ventilation, Renew. Energy 35 (2010) 2080–2088.
[6] H.W. Jing, Z.D. Chen, A.G. Li, Experimental study of the prediction of the ventilation flow rate through solar chimney with large gap-to-height ratios, Build. Environ. 89 (2015) 150–159.
[7] L. Shi, M.Y.L. Chew, A review on sustainable design of renewable energy systems, Renew. Sustain. Energy Rev. 16 (2012) 192–207.
[8] Z.D. Chen, P. Bandopadhayay, J. Halldorsson, C. Byrjalsen, P. Heiselberg, Y. Li, An experimental investigation of a solar chimney model with uniform wall heat flux, Build. Environ. 38 (2003) 893–906.
[9] A.Y.K. Tan, N.H. Wong, Natural ventilation performance of classroom with solar chimney system, Energy Build. 53 (2012) 19–27.
[10] K. Pavlou, K. Vasilakopoulou, M. Santamouris, The impact of several construction elements on the thermal performance of solar chimneys, Int. J. Vent. 8 (2009) 277–285.
[11] K.E. Amori, S.W. Mohanmmed, Experimental and numerical studies of solar chimney for natural ventilation in Iraq, Energy Build. 47 (2012) 450–457.
[12] D.S. Lee, T.C. Hung, J.R. Lin, J. Zhao, Experimental investigations on solar chimney for optimal heat collection to be utilized in organic Rankine cycle, Appl. Energy 154 (2015) 651–662.
[13] C. Afonso, A. Oliveira, Solar chimneys: simulation and experiment, Energy Build. 32 (2000) 71–79.
[14] J. Arce, M.J. Jimenez, J.D. Guaman, M.R. Heras, G. Alvarez, J. Xaman, Experimental study for natural ventilation on a solar chimney, Renew. Energy 34 (2009) 2928–2934.
[15] K.T. Andersen, Thoery for natural ventilation by thermal buoyancy in one zone with uniform temperature, Build. Environ. 38 (2003) 1281–1289.
[16] N.K. Bansal, R. Mathur, M.S. Bhandari, Solar chimney for enhanced stack ventilation, Build. Environ. 28 (1993) 373–377.
[17] R. Bassiouny, N.S.A. Korah, Effect of solar chimney inclination angle on space flow pattern and ventilation rate, Energy Build. 41 (2009) 190–196.
[18] F. Flourentzou, J. Van der Maas, C.A. Roulet, Natural ventilation for passive cooling: measurement of discharge coefficients, Energy Build. 27 (1998) 283–292.
[19] E.P. Sankonidou, T.D. Karapantsios, A.I. Balouktsis, D. Chassapis, Modeling of the optimum tilt of a solar chimney for maximum air flow, Sol. Energy 82 (2008) 80–94.
[20] J. DeBlois, M. Bilec, L. Schaefer, Simulating home cooling load reductions for a novel opaque roof solar chimney configuration, Appl. Energy 112 (2013) 142–151.
[21] G.H. Gan, Impact of computational domain on the prediction of buoyancy-driven ventilation cooling, Build. Environ. 45 (2010) 1173–1183.
[22] A.A. Imran, J.M. Jalil, S.T. Ahmed, Induced flow for ventilation and cooling by a solar chimney, Renew. Energy 78 (2015) 236–244.
[23] Q.Y. Chen, Ventilation performance prediction for buildings: a method overview and recent applications, Build. Environ. 44 (2009) 848–858.
[24] E. Bacharoudis, M.G. Vrachopoulos, M.K. Koukou, D. Margaris, A.E. Filios, S.A. Mavrommatis, Study of the natural convection phenomena inside a wall solar chimney with one wall adiabatic and one wall under a heat flux, Appl. Therm. Eng. 27 (2007) 2266–2275.
[25] A. Acred, G.R. Hunt, A simplified mathematical approach for modelling stack ventilation in multi-compartment buildings, Build. Environ. 71 (2014) 121–130.
[26] K. McGrattan, S. Hostikka, R. McDermott, J. Floyd, C. Weinschenk, K. Overholt, Fire Dynamics Simulator User's Guide, 1019, U.S. National Institute of Standards and Technology, NIST Special Publication, 2015.
[27] A. Bystrom, X.D. Cheng, U. Wickstrom, M. Veljkovic, Full-scale experimental and numerical studies on compartment fire under low ambient temperature, Build. Environ. 51 (2012) 255–262.
[28] W.K. Chow, S.S. Li, Y. Gao, C.L. Chow, Numerical studies on atrium smoke movement and control with validation by field tests, Build. Environ. 44 (2009) 1150–1155.
[29] J. Floyd, Coupling a network HVAC Model to a computational fluid dynamics model using large eddy simulation, Fire Saf. Sci. 10 (2011) 459–470.
[30] J. Wahlqvist, P. van Hees, Validation of FDS for large-scale well-confined mechanically ventilated fire scenarios with emphasis on predicting ventilation system behavior, Fire Saf. J. 62 (2013) 102–114.
[31] K. McGrattan, S. Hostikka, R. McDermott, J. Floyd, C. Weinschenk, K. Overholt, Fire Dynamics Simulator Technical Reference Guide Volume 1: Mathematical Model, U.S. National Institute of Standards of Technology, NIST Special Publication 1018-1, 2015.
[32] A. Bouchair, Solar Induced Ventilation in the Algerian and Similar Climates, PhD Thesis, University of Leeds, UK, 1989.
[33] K. McGrattan, S. Hostikka, R. McDermott, J. Floyd, C. Weinschenk, K. Overholt, Fire Dynamics Simulator Technical Reference Guide Volume 3: Validation, National Institute of Standards and Technology, NIST Special Publication 1018-3, 2015.
[34] F. Kreith, R.M. Manglik, M.S. Bohn, Principles of Heat Transfer, seventh ed., Cengagae Learning, 2011.
[35] S. Obyn, G. van Moeseke, Variability and impact of internal surfaces convective heat transfer coefficients in the thermal evaluation of office buildings, Appl. Therm. Eng. 87 (2015) 258–272.
[36] J.P. Abraham, E.M. Sparrow, Experiments on discretely heated, vented/unvented enclosures for various radiation surface characteristics of the thermal load, enclosure temperature sensor, and enclosure walls, Int. J. Heat. Mass Transf. 45 (2002) 2255–2263.
[37] K.T. Andersen, Theoretical considerations on natural ventilation by thermal buoyancy, ASHRAE Trans. 101 (1995) 1103–1117.
[38] X.Q. Zhai, Y.J. Dai, R.Z. Wang, Experimental investigation on air heating and natural ventilation of a solar air collector, Energy Build. 37 (2005) 373–381.
[39] R. Bassiouny, N.S.A. Koura, An analytical and numerical study of solar chimney use for room natural ventilation, Energy Build. 40 (2008) 865–873.
[40] D.J. Harris, N. Helwig, Solar chimney and building ventilation, Appl. Energy 84 (2007) 135–146.